# PEGylated Nanoparticles Bind to and Alter Amyloid-Beta Peptide Conformation: Toward Engineering of Functional Nanomedicines for Alzheimer's Disease

**Davide Brambilla,[†] Romain Verpillot,[†] Benjamin Le Droumaguet,[†] Julien Nicolas,[†] Myriam Taverna,[†] Juraj Kóňa,[‡] Barbara Lettiero,[§] S. Hossein Hashemi,[§] Line De Kimpe,[⊥] Mara Canovi,[∥] Marco Gobbi,[∥] Valérie Nicolas,[¶] Wiep Scheper,[⊥] S. Moein Moghimi,[§,#] Igor Tvaroška,[‡] Patrick Couvreur,[†] and Karine Andrieux[†,*]**

[†]Laboratoire de Physico-Chimie, Pharmacotechnie et Biopharmacie, UMR CNRS 8612, Univ Paris-Sud 11, Faculté de Pharmacie, 5 rue Jean-Baptiste Clément, F-92296 Chatenay-Malabry, France, [‡]Institute of Chemistry, Center for Glycomics, Slovak Academy of Sciences, Dúbravska cesta 9, 845 38 Bratislava, Slovakia, [§]Nanomedicine Laboratory, Centre for Pharmaceutical Nanotechnology and Nanotoxicology, University of Copenhagen, Universitetsparken 2, DK-2100 Copenhagen Ø, Denmark, [⊥]Department of Genome Analysis, Academic Medical Center, University of Amsterdam, 1012 WX Amsterdam, The Netherlands, [∥]Istituto di Ricerche Farmacologiche "Mario Negri", 20156 Milano, Italy, [¶]Institut d'Innovation Thérapeutique (IFR141 ITFM), Univ Paris-Sud, Faculté de Pharmacie, 5 rue Jean-Baptiste Clément, F-92296 Châtenay-Malabry, France, and [#]NanoScience Centre, University of Copenhagen, DK-2100 Copenhagen Ø, Denmark

**ABSTRACT** We have demonstrated that the polyethylene glycol (PEG) corona of long-circulating polymeric nanoparticles (NPs) favors interaction with the amyloid-beta ($A\beta_{1-42}$) peptide both in solution and in serum. The influence of PEGylation of poly(alkyl cyanoacrylate) and poly(lactic acid) NPs on the interaction with monomeric and soluble oligomeric forms of $A\beta_{1-42}$ peptide was demonstrated by capillary electrophoresis, surface plasmon resonance, thioflavin T assay, and confocal microscopy, where the binding affected peptide aggregation kinetics. The capture of peptide by NPs in serum was also evidenced by fluorescence spectroscopy and ELISA. Moreover, *in silico* and modeling experiments highlighted the mode of PEG interaction with the $A\beta_{1-42}$ peptide and its conformational changes at the nanoparticle surface. Finally, $A\beta_{1-42}$ peptide binding to NPs affected neither complement activation in serum nor apolipoprotein-E (Apo-E) adsorption from the serum. These observations have crucial implications in NP safety and clearance kinetics from the blood. Apo-E deposition is of prime importance since it can also interact with the $A\beta_{1-42}$ peptide and increase the affinity of NPs for the peptide in the blood. Collectively, our results suggest that these engineered long-circulating NPs may have the ability to capture the toxic forms of the $A\beta_{1-42}$ peptide from the systemic circulation and potentially improve Alzheimer's disease condition through the proposed "*sink effect*".

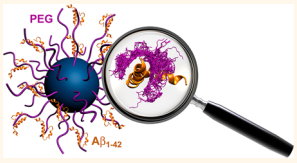


**KEYWORDS:** polyethylene glycol · nanoparticles · $A\beta_{1-42}$ · binding · Alzheimer's disease

Alzheimer's disease (AD) is the most common form of senile dementia affecting more than 35 million people worldwide. This neurodegenerative disorder, clinically characterized by a progressive loss of memory and other cognitive abilities, can be identified by different physiopathological hallmarks such as neuronal loss, glial proliferation, extracellular amyloid plaque deposition mainly composed of amyloid-beta peptide ($A\beta$), and intracellular neurofibrillary tangles of hyperphosphorylated $\tau$-protein.[1] AD is likely the result of a multifactorial process in which genetic and environmental factors are involved. The etiology of the disease is still under debate.[2] AD treatment constitutes a major challenge in medicine as all current therapies are restricted to AD symptom alleviation.

Progressive production, accumulation, and aggregation of $A\beta$ peptide leads to the formation of amyloid plaques in the brain.[3,4] $A\beta$ peptide is produced by numerous cells such as neurons from the proteolysis of amyloid precursor protein (APP). In AD patients, APP is cleaved by $\beta$- and $\gamma$-secretases forming $A\beta$ fragments with varying number of amino acids ranging from 36 to 42.[5,6] Although the origin of the $A\beta$ peptide that accumulates in the brain is still unclear,[7] the peptide can leave the brain by crossing the blood–brain barrier (BBB) with the aid of transport molecules such as apolipoprotein-E2/3 (Apo-E2/3) and Apo-E4 through two efflux pumps, the lipoprotein receptor-related protein (LRP) and the very low density lipoprotein receptor (VLDLR).[8–10] Under pathological conditions, the clearance of $A\beta$ peptide from the body seems dramatically reduced, which may be related to an age-dependent decline of peptide degradation enzymes expression in the brain, thus leading to a progressive peptide accumulation and aggregation in

* Address correspondence to karine.andrieux@u-psud.fr.

Received for review February 2, 2012 and accepted June 11, 2012.

**Published online June 11, 2012**
10.1021/nn300489k

**TABLE 1. Physico-Chemical Properties of the Nanoparticles Used in Experiments**

| | PHDCA[a] | P(MePEGCA-*co*-RCA-*co*-HDCA)[a] | P(MePEGCA-*co*-HDCA)[a] | PLA[a] | PLA-*b*-PEG[a] |
|---|---|---|---|---|---|
| mean diameter[b] (nm) | 163 ± 3 | 98 ± 3 | 91 ± 3 | 105 ± 1 | 110 ± 3 |
| polydispersity index[b] | 0.11 | 0.23 | 0.14 | 0.22 | 0.21 |
| zeta-potential (mV) | −26 ± 7 | −35 ± 3 | −30 ± 5 | −10 ± 4 | −15 ± 5 |
| PEG distance[c] (nm) | | 1.21 | 1.21 | | 0.91 |

[a] PACA family: PHDCA, poly(hexadecyl cyanoacrylate); P(MePEGCA-*co*-RCA-*co*-HDCA), poly[(hexadecyl cyanoacrylate)-*co*-rhodamine B cyanoacrylate-*co*-methoxypoly(ethylene glycol)$_{2000}$ cyanoacrylate]; P(MePEGCA-*co*-HDCA), poly[(hexadecyl cyanoacrylate)-*co*-methoxypoly(ethylene glycol)$_{2000}$ cyanoacrylate]. PLA family: PLA, poly(lactic acid); PLA-b-PEG, poly(lactic acid)-*b*-poly(ethylene glycol)$_{2000}$. [b] Determined by dynamic light scattering. [c] Theoretical distance between adjacent PEG chains measured as described in the Materials and Experiments section.

small oligomers, soluble $\beta$-sheet aggregates, fibrils, and finally plaques.[11,12] Among the different species, the A$\beta$ peptide 1−42 (A$\beta_{1-42}$) monomer is considered the most toxic isoform due to its higher tendency to aggregate,[13,14] whereas the soluble A$\beta_{1-42}$ oligomer is toxic to neurons.[15,16] In this context, a great deal of effort has been devoted to the development of interventions capable of interacting with A$\beta$ peptide at different steps of its aggregation pathway in order to either (*i*) favor its elimination, thereby reaching the equilibrium between production and clearance; or (*ii*) slow down the aggregation process.[17−19]

PEGylated long-circulating nanoparticles (NPs) of poly(alkyl cyanoacrylate) (PACA) and poly(lactic acid) (PLA) (co)polymers have long been used for targeted drug delivery due to their favorable pharmacokinetics and biocompatibility properties.[20,21] These NPs are currently in clinical trials for the treatment of multidrug resistance (MDR) hepatocarcinoma (phase III) and prostate cancer (phase I), respectively.[22,23] It has been shown that the PEG corona of PACA NPs favors selective adsorption of Apo-E.[24,25] Accordingly, they may serve as promising platforms in binding and capturing circulating A$\beta_{1-42}$ peptide from the blood and redirecting the peptide to the hepatic macrophages for destruction.

In this work, we performed *in vitro* and *in silico* experiments to study this possibility and report on the remarkable properties of these nanoparticles in A$\beta_{1-42}$ peptide binding and conformational changes.

## RESULTS AND DISCUSSION

The interaction of A$\beta_{1-42}$ peptide with NPs of different compositions and properties (Table 1) as well as free PEG molecules was investigated by a range of state-of-the-art techniques. These included capillary electrophoresis with fluorescence or UV detector (CE-LIF/UV), surface plasmon resonance (SPR), thioflavin T assay, confocal laser scanning microscopy (CLSM), and molecular modeling.

A PEG chain length of 2000 Da has been selected as a compromise between copolymer hydrophobicity, blood opsonin repulsion, and affinity for A$\beta_{1-42}$ peptide. We noticed a decrease in the zeta-potential value of PHDCA nanoparticles when they were PEGylated (Table 1); this feature may be attributed to the presence of rhodamine moieties in the polymer structure, which are likely exposed at the nanoparticle surface.[26]

**Monitoring of NP Interaction with A$\beta_{1-42}$ Monomers by Capillary Electrophoresis.** Earlier we established the application of capillary electrophoresis coupled with laser-induced fluorescence detection (CE-LIF) to monitor and quantify the interaction between NPs and the monomeric form of the A$\beta_{1-42}$ peptide.[27] We have now extended these studies to investigate the kinetics of A$\beta_{1-42}$ "disappearance" in the presence of two classes of PEGylated polymeric NPs (*i.e.*, PACA and PLA) and their non-PEGylated counterparts. The peak associated with the monomeric form of A$\beta_{1-42}$ peptide (expressed as the % of the initial peptide concentration) was monitored as a function of time (Figure 1). At a concentration of 5 $\mu$M, the peptide maintained its monomeric state during the whole CE analysis as no significant changes in the peptide peak were observable (Figure 1c). Interestingly, in the presence of poly[methoxypoly(ethylene glycol) cyanoacetate-*co*-rhodamine B cyanoacetate-*co*-hexadecyl cyanoacetate] (P(MePEGCA-*co*-RCA-*co*-HDCA)) NPs, a dramatic decrease in the peptide peak intensity was observed, whereas the amount of the free peptide monomer in the analysis buffer remained unchanged when non-PEGylated poly(hexadecyl cyanoacrylate) (PHDCA) NPs were added (Figure 1a).

In the case of PEGylated and non-PEGylated PLA NPs, a decrease in the peptide monomer peak was recorded (Figure 1b). In contrast to PHDCA NPs, PLA NPs were able to bind the peptide monomer. However, nanoparticle PEGylation clearly favored interaction with the A$\beta_{1-42}$ peptide. Even PEG ($M_n$ = 2 kDa, Figure 1c) in free form showed tendency to interact with A$\beta_{1-42}$ peptide, resulting in aggregate formation. Notably, within the first 3 h, the monomer peptide peak remained unchanged, thus suggesting a lag phase before initiation of peptide aggregation.

All tested samples, with the exception of PHDCA NPs, showed affinity for the monomeric A$\beta_{1-42}$ peptide but with different kinetics. The following binding order of P(MePEGCA-*co*-RCA-*co*-HDCA) NPs > PEG-*b*-PLA NPs > free PEG > PLA NPs highlights the importance of the surface-projected PEG chains on peptide

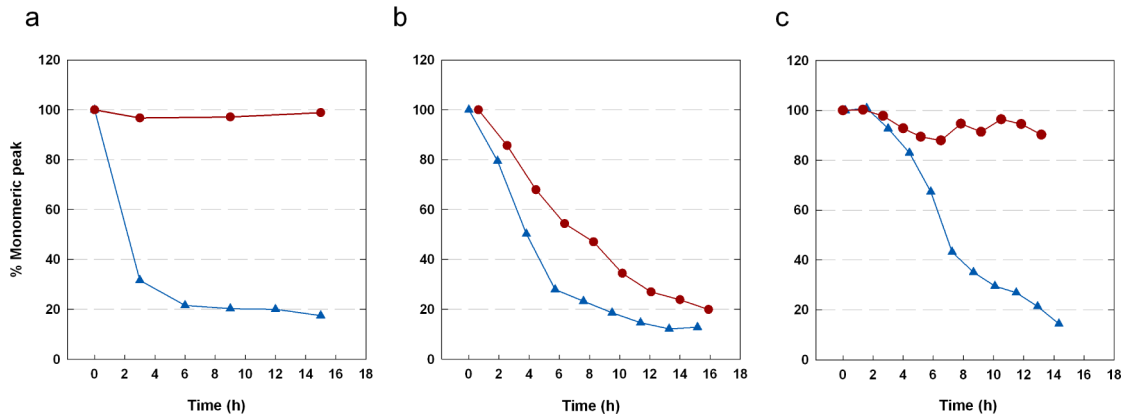


**Figure 1. Evolution of the A$\beta_{1-42}$ peptide monomer peak intensity as a function of time at 37 °C monitored by CE-LIF experiments. (a) Represents 5 $\mu$M Hilyte Fluor A$\beta_{1-42}$ in the presence of 20 $\mu$M rhodamine-labeled P(MePEGCA-*co*-RCA-*co*-HDCA) (▲) or PHDCA nanoparticle suspension (●); (b) kinetic profile of 5 $\mu$M Hilyte Fluor A$\beta_{1-42}$ in the presence of 20 $\mu$M PEG-PLA (▲) or PLA (●) nanoparticle suspension; and (c) profile of 5 $\mu$M Hilyte Fluor A$\beta_{1-42}$ solution alone (●) and in the presence of 20 $\mu$M free 2 kDa MePEG (▲).**

immobilization. The faster peptide binding kinetics observed with PEGylated NPs compared with free PEG molecules (used at the same concentration as for the copolymers) could be indicative of a multistep process. In the first step, multiple and cooperative interactions between the peptide monomer and the immobilized PEG chains could dramatically increase the localized peptide concentration at the NP surface, thereby triggering its aggregation. Accordingly, this may explain the fast binding step without any lag phase, indicating that PEGylated NPs are superior than free PEG molecules for capturing and eliminating this peptide. Previous experiments have highlighted that the size, the surface charge, and the nature of the surfactant used for NP preparation can have a strong influence on their affinity for the A$\beta_{1-42}$ peptide monomer.[28] The present study shows that NP core and shell both contribute to A$\beta_{1-42}$ peptide binding. However, the adsorption of A$\beta_{1-42}$ peptide on PEGylated NPs is predominantly PEG-based. Finally, among the tested NPs, P(MePEGCA-*co*-RCA-*co*-HDCA) species appeared to be the most promising entities for potential treatment of AD pathology due to their high propensity to capture the peptide monomer (80% of monomers have disappeared after 6 h) as well as their established prolonged circulation times in the blood. This is of significance since earlier studies have shown that at 6 h post-intravenous injection, 0.3 and 30% of the dose of PHDCA and P(MePEGCA-*co*-HDCA) NPs remains in the blood, respectively.[29] Because a PEGylated NP concentration of 0.5 mM could be achieved in plasma at this time, our *in vitro* experiments performed at a NP concentration of 20 $\mu$M could correspond to preclinical doses. So P(MePEGCA-*co*-HDCA) NPs appear to be well-suited for potential AD therapy.

**Monitoring of NP-A$\beta_{1-42}$ Peptide Monomer Interaction by SPR.** To further investigate the affinity of P(MePEGCA-*co*-HDCA) NPs for A$\beta_{1-42}$ peptide, the binding properties of PEGylated and non-PEGylated PACA NPs with A$\beta_{1-42}$ monomers were then evaluated by SPR experiments. The results confirm the affinity of flowing P(MePEGCA-*co*-HDCA) NPs at concentrations greater than 3 $\mu$M for immobilized peptide monomers (Figure 2a). The binding of PEGylated PACA NPs was increasing with their concentration and was specific for A$\beta_{1-42}$ since no binding was observed in parallel on an empty surface or on a surface immobilizing BSA (Figure S1 in Supporting Information). In contrast, no binding was observed between PHDCA NPs and the peptide even at higher NP concentrations (20 $\mu$M, Figure 2b).

Through SPR experiments (Figure S2), we further established a $k_d$ value of 161 $\mu$M (based on NP concentration) for A$\beta_{1-42}$ monomers and rhodamine B-tagged fluorescent P(MePEGCA-*co*-RCA-*co*-HDCA) NPs, thus confirming the affinity of PEGylated NPs for the monomeric form of the peptide. The SPR-derived $k_d$ value was higher than that obtained by CE-LIF experiments (0.55 $\mu$M).[27] This may be assigned to the intrinsic differences between the two techniques. Peptide immobilization can presumably reduce the number of available binding sites to the flowing NPs. Accordingly, the SPR may underestimate the $k_d$ value. In addition in CE-LIF experiments, the peptide employed bears a covalently attached fluorophore that may slightly influence the $k_d$.

**Monitoring of NP and A$\beta_{1-42}$ Interaction by Thioflavin T Assay and Microscopy.** An established thioflavin T (ThT) assay was also used to monitor NP-induced A$\beta_{1-42}$ peptide aggregation through the $\beta$-sheet formation pathway. The peptide/NP molar ratio was tuned from 1/2 to 1/4, and the fluorescence intensity, arising from ThT affinity for the $\beta$-sheets in A$\beta$ peptide aggregates, was measured at different incubation times (Figure 3). ThT experiments were performed at higher peptide concentration (*i.e.*, 50 $\mu$M) than for CE experiments in order to favor the formation of $\beta$-sheet. Time-dependent

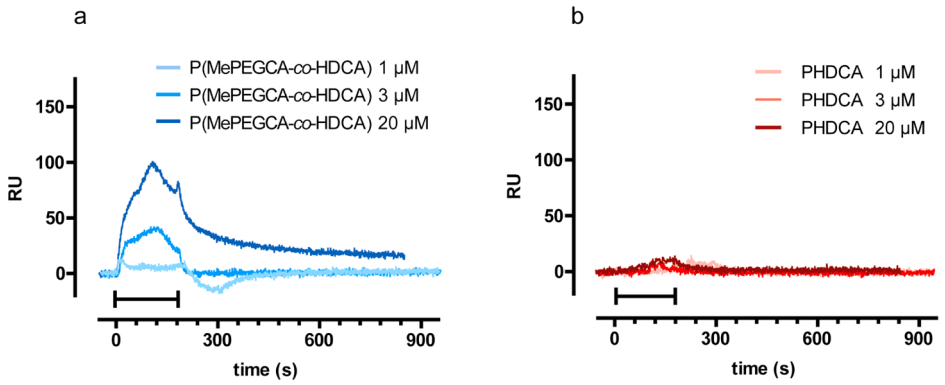


**Figure 2. Surface plasmon resonance sensorgrams of (a) P(MePEGCA-*co*-HDCA) NPs and (b) PHDCA NP interaction with A$\beta_{1-42}$ monomers immobilized on the sensor chip.**

aggregation was observed with the peptide alone through an increase of the fluorescence intensity (Figure 3). After incubation with NPs and regardless of the A$\beta_{1-42}$/NP molar ratio (Figure 3), PHDCA NPs had no effect on peptide aggregation kinetics, whereas P(MePEGCA-*co*-HDCA) NPs strongly increased $\beta$-sheet formation, thus supporting a role for PEG in peptide aggregation.

The interaction between A$\beta_{1-42}$ peptide (10 $\mu$M) and NPs (20 $\mu$M) was further evaluated by confocal microscopy (Figure S3). The results confirmed the ability of PEGylated NPs to sequester the peptide and favor its aggregation. Therefore, it is likely that the peptide aggregation, which was observed with both techniques, is initiated or increased after capture by the outer PEG shell of the NPs acting as an aggregation initiator.

**NP Influence on A$\beta_{1-42}$ Aggregation by Capillary Electrophoresis.** In order to have an in-depth insight of the influence of PEGylated NPs on the peptide aggregation, a new CE protocol was developed. An aggregated solution (50 $\mu$M) of nonlabeled A$\beta_{1-42}$, obtained by adapting a protocol previously described,[30] was mixed with thioflavin, and the sample was analyzed by CE-LIF as a function of incubation time at 37 °C. Prior to the analysis in the presence of NPs, ThT analysis was employed to confirm the formation of $\beta$-sheet in solution. The fluorescence measurements confirmed the formation of typical amyloid soluble oligomers (Figure S4). Then, NPs were added to a solution of aggregating A$\beta_{1-42}$ peptide, and the formation/disappearance of A$\beta_{1-42}$ monomer and soluble oligomers was monitored and quantified by CE coupled to a UV detector. A freshly prepared stock solution of peptide was employed as the control experiment. The analysis of this control showed a reduction of monomeric forms, concomitantly, with an increase of oligomeric form over the time and in good agreement with the peptide aggregation mechanism (Figure 4a). However, when the aggregating solution of peptide was incubated with NPs, three main differences were observed when compared with the peptide alone: (*i*) a faster decrease of the monomer peak, (*ii*) a sharp decrease (almost entirely eliminated) of the oligomer

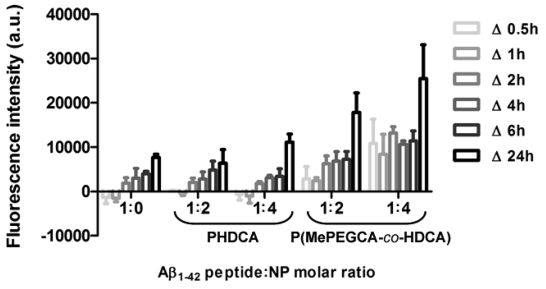


**Figure 3. ThT assay for monitoring A$\beta_{1-42}$ peptide aggregation. A$\beta_{1-42}$ (50 $\mu$M) was incubated in the presence of P(MePEGCA-*co*-HDCA) or PHDCA NPs at different peptide/NP molar ratios for 24 h at 37 °C. At the indicated time points, aliquots were taken to analyze the $\beta$-sheet content by the ThT assay. The bars represent the absolute change in fluorescence for different time slots. The graph shows the mean ± SD ($n$ = 3) of three independent experiments.**

species (7.8 and 9.25 min) present at the onset of the kinetics, and (*iii*) the appearance of "spike-shape" peaks likely due to the formation of bigger aggregates networked with NPs *via* A$\beta$ oligomeric bridges (Figure 4b).

These results clearly demonstrated the ability of the PEGylated NPs not only to capture the peptide monomer and its soluble oligomers in solution but also to inhibit the formation of new soluble peptide oligomers (*i.e.*, disappearance of the peak at 9.25 min). Indeed, 75% of the pre-existing soluble oligomers were no longer detectable in the solution after 28 h of incubation, whereas in the absence of NPs, 80% increase of peptide oligomers was observed after 28 h (Figure 5).

**Molecular Modeling Experiments.** In order to investigate the nature of the interactions between the PEG chains and the A$\beta_{1-42}$ monomer, as well as their consequences on the conformation of the peptide, molecular modeling experiments were performed (Figures 6 and 7). For comparison, the dynamics of the polyethylene (PE) chain, which is exclusively hydrophobic, was also computed in the presence of the peptide.

The docking calculations were performed (*i*) to build a starting geometry of the model nanoparticle–peptide complexes and (*ii*) to analyze interactions between PEG (or PE) units and amino acid residues of

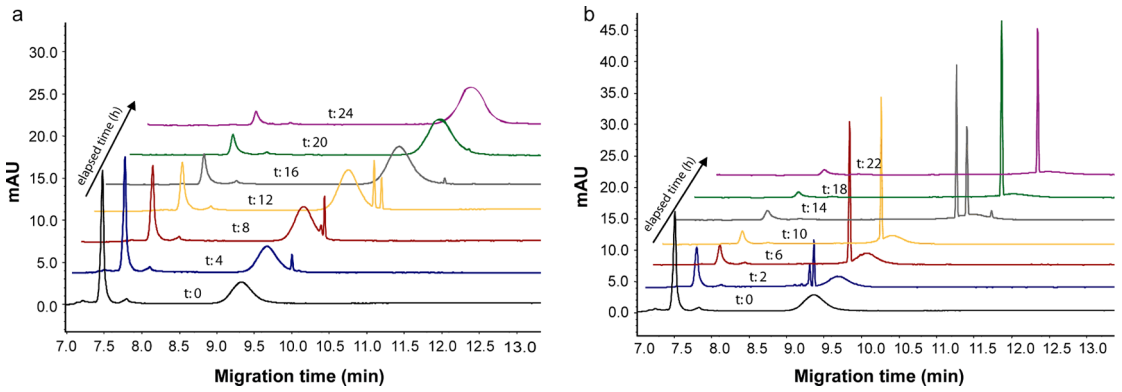


**Figure 4. CE-UV monitoring of peptide A$\beta_{1-42}$ aggregation. Evolution of the peak intensity of peptide monomers and oligomers as a function of time at 37 °C of a 50 $\mu$M A$\beta_{1-42}$ solution alone (a) and in the presence of a 20 $\mu$M P(MePEGCA-*co*-HDCA) NP suspension (b).**

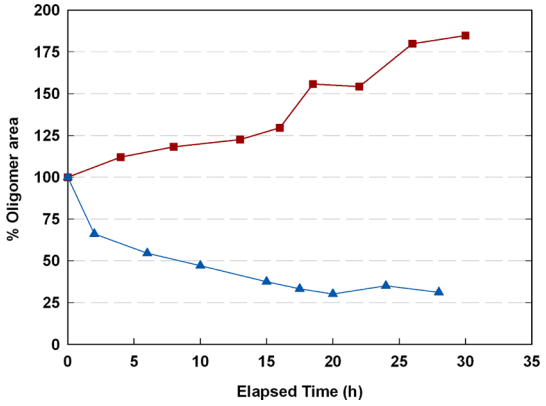


**Figure 5. Quantification of oligomer peak (migration time = 9.25 min; see Figure 4) as function of time at 37 °C of 50 $\mu$M A$\beta_{1-42}$ solution alone and in the presence of 20 $\mu$M P-(MePEGCA-*co*-HDCA) NP suspension.**

the peptide. The structural analysis of docked poses of the PEG chain at A$\beta_{1-42}$ indicated that the polymeric fragment was capable of binding the peptide in a nonspecific manner (Figure 6a). It wound around the helix (1−25) of the peptide, preferably to the sequence between the His13 and Gly25 residues. In Figure 6b, 50 poses of the docked PEG chain with the best docking score were visualized. Interestingly, PEG preferably wound around the helix (1−25) and interacted partially with the helix (26−42) at the turn between the helices. The interaction was mediated by the oxygen atoms either with the polar (or basic) side chains of His13, Lys28, Lys16, or Gln15 (hydrogen bonds) or with the hydrophobic chains of Phe19, Phe20 ($\pi$-stack interactions), and Val24, Ile31, Leu34, or Met35 (van der Waals interactions). To evaluate the role of PEG oxygen atoms on peptide binding, the alkyl PE chain was also docked to the peptide (Figure 6c) for comparison. The alkyl chain did not wind around the helix (1−25) and interacted only with terminal parts of both helices (1−25) and (26−42). The measured weak binding of the alkyl chain to the peptide was also supported by a docking score, which was in the range of (−1.51) to (+0.98) kcal mol$^{-1}$ starting from the best pose to the 50th pose of the ligand. For comparison, the docking score of the PEG chain ranged from (−3.68) to (−0.24) kcal mol$^{-1}$. This clearly indicated the importance of the oxygen atoms of PEG in A$\beta_{1-42}$ peptide−NP interaction.

Next, the molecular dynamics simulations were performed to evaluate whether permanent interactions between the PEG chain and A$\beta_{1-42}$ could occur and to analyze conformational changes of the bound peptide. The starting geometry of A$\beta_{1-42}$ taken from the crystal structure was characterized by two α-helical regions (sequences 15−25 and 31−39) connected by a flexible link. During the simulation with the PEG chain, these helices were partially disrupted and then again partially restored into shorter sequences (19−22 and 31−34) (Figure 7a). In contrast, in the presence of the hydrophobic PE chain, the region of the α-helix (15−25) was maintained in its initial conformation (Figure 7b). The other α-helix (31−39) was disrupted at the beginning of the simulation but restored at the end. It seemed that in the presence of the hydrophobic PE chain, the peptide maintained more easily its helical character and was more resistant to conformational changes because the helical structures of the peptide were transformed into smaller helical fragments separated by turns and coils. The most intensive conformational changes of A$\beta_{1-42}$ in the presence of the PEG chain were evident from the calculated root-mean-square deviation (rmsd) of the Cα carbons of the backbone of A$\beta_{1-42}$ during the simulations (Figure S5). The rmsd for the system with the PEG chain was higher compared to that with the PE chain. Conformational changes of A$\beta_{1-42}$ produced the conversion of the starting L-like shape structure of the peptide to V-like, U-like shapes, or even more complex conformations. The main feature of the conformational interconversion of A$\beta_{1-42}$ was a permanent interaction with the PEG chain. The permanent interaction of the peptide with the polymeric chain was also observed for the system with the PE chain. However, this interaction slowed down conformational changes and stabilized

**Figure 6. *In silico* modeling of PEG-A$\beta_{1-42}$ interaction modes. (a) PEG chain (vdW) docked to A$\beta_{1-42}$ (surfaces). The chain interacts with both hydrophobic as well as hydrophilic residues of the peptide and forms a spiral structure. (b) Best 50 poses of the PEG chain (purple) docked to A$\beta_{1-42}$ (orange), and (c) alkyl PE chain (purple) docking on A$\beta_{1-42}$ (orange).**

the peptide in its α-helical conformation. Both PEG and PE chains showed high flexibility during the simulations, changing their shapes from several linear conformations wound around A$\beta_{1-42}$ into partially packed structures of different shapes inside the U-like or more complex shapes of A$\beta_{1-42}$.

In summary, the molecular modeling experiments highlighted the mode of interactions (forces, residues, and conformational changes) between the PEG shell of nanoparticles and the A$\beta_{1-42}$ monomer and supported the conformation change of the peptide (bound at the surface of the NPs) observed during ThT assay and confocal microscopy experiments.

**Complement Activation by Selected NPs.** Complement activation and fixation is a fundamental process contributing to macrophage clearance of intravenously injected NPs. Accordingly, complement activation studies in human serum were performed with P(MePEGCA-*co*-HDCA) NPs before and after A$\beta_{1-42}$ peptide binding. Surface peptide deposition had no significant effect on the level of complement activation products C4d, Bb, C5a, and SC5b-9 (Figure 8). With both systems, only a slight level of complement activation was observable compared with positive controls (aggregated IgG and Zymosan). On the basis of these results, we anticipate that A$\beta_{1-42}$ peptide-bound nanoparticles may exhibit blood clearance kinetic profiles similar to that of native nanoparticles, thus aiding peptide localization to the macrophages of the reticuloendothelial system for destruction and further processing.

**A$\beta_{1-42}$ Peptide−NP Interaction in Serum.** We further evaluated whether the PEGylated NPs could capture and eliminate A$\beta_{1-42}$ peptides from serum. For this purpose, PEGylated and nonstealth NPs were incubated in fetal bovine serum (FBS) in the presence of either fluorescently labeled or nonlabeled peptide at 37 °C. At 7 h post-incubation, NPs were removed by centrifugation and the remaining peptide in the supernatant was quantified either by fluorescence spectroscopy or by ELISA.

Both the fluorescence analysis and the ELISA assay confirmed the ability of PEGylated NPs to capture the peptide from serum. For instance, fluorescence

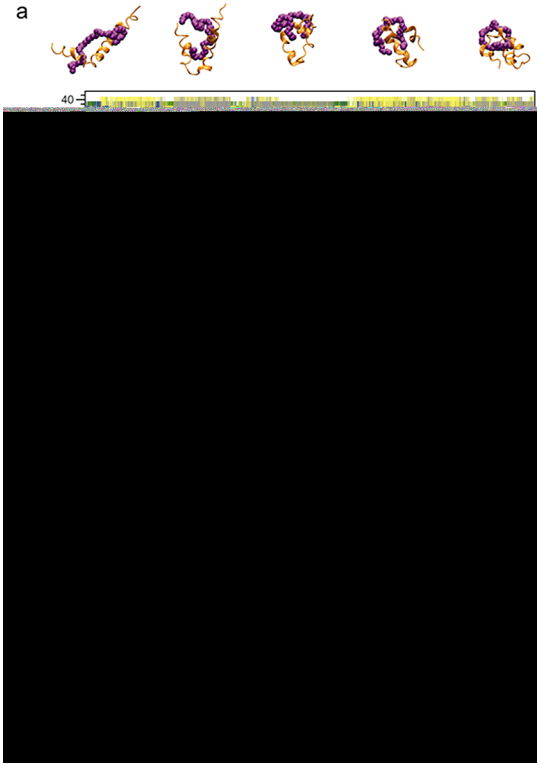


**Figure 7. Molecular dynamic simulation experiments. Changes of the secondary structure of A$\beta_{1-42}$ for the complexes (a) PEG/A$\beta_{1-42}$ and (b) PE/A$\beta_{1-42}$ during 20 ns of simulation. PEG and PE chains are visualized in purple and A$\beta_{1-42}$ in orange.**

spectroscopy showed that P(MePEGCA-*co*-HDCA) NP treatment could significantly decrease the amount of soluble peptide in serum comparatively to the control NPs (Figure 9a). The reduction in serum levels of A$\beta_{1-42}$ peptide was shown to be 15% of total peptide bound to PEGylated NPs (Figure 9b).

**Apo-E Adsorption on Selected NPs in the Presence of A$\beta_{1-42}$ Peptide.** Previous experiments using 2D-PAGE analysis and Western blots have demonstrated the adsorption of Apo-E onto the surface of P(MePEGCA-*co*-HDCA) NPs from serum.[24] Accordingly, we monitored Apo-E adsorption to NPs in serum supplemented with A$\beta_{1-42}$ peptide (Figure 10). The results confirmed Apo-E adsorption, thus suggesting that the binding of A$\beta$ peptide has no significant effect on further protein

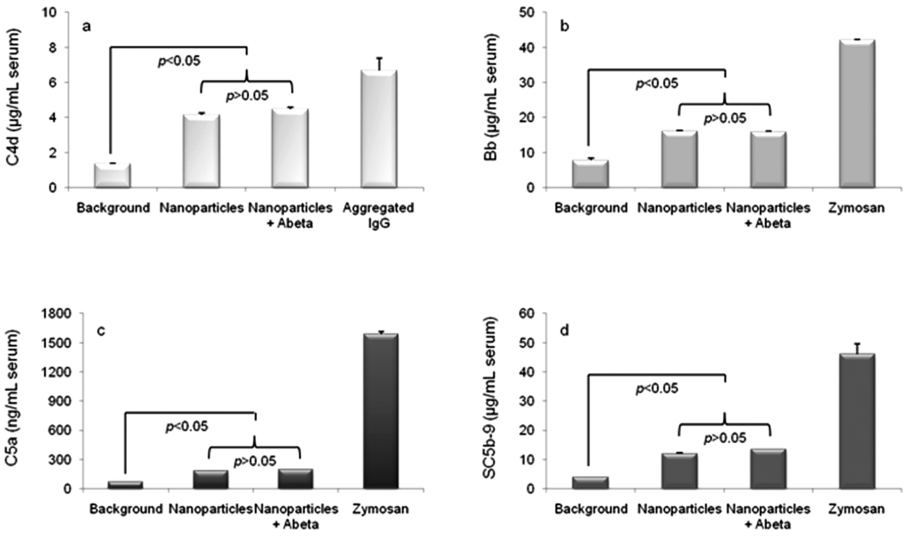


**Figure 8. Complement activation. Quantification of complement activation products, (a) C4d, (b) Bb, (c) C5a, and (d) SC5b-9, in healthy human serum after incubation of P(MePEGCA-*co*-HDCA) nanoparticles with or without A$\beta_{1-42}$ peptide preadsorption step. Background and positive control (aggregated IgG or Zymosan) are presented for each product.**

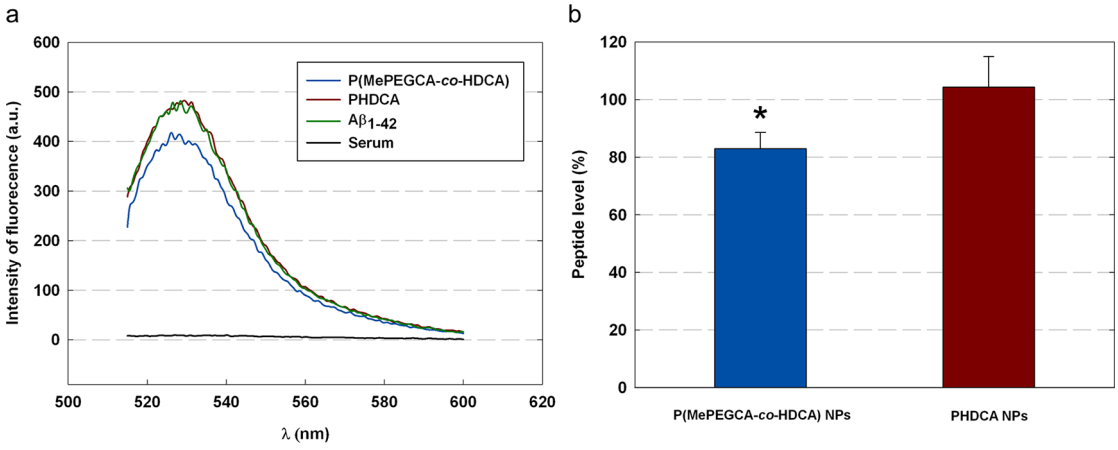


**Figure 9. Qualitative and quantitative determination of the A$\beta_{1-42}$ peptide capture by P(MePEGCA-*co*-HDCA) and PHDCA NPs from serum. (a) Fluorescence spectroscopy was used to monitor peptide disappearance from serum (controls corresponded to peptide alone (A$\beta_{1-42}$) and to serum), and (b) ELISA was used to quantify peptide binding to NPs ($n$ = 3). Statistical difference is expressed by * ($p$ < 0.05).**

binding. Since Apo-E is known to interact with the A$\beta_{1-42}$ peptide *in vivo*, its adsorption on NPs could further increase the peptide affinity for NPs and hence its elimination from the circulation. Therefore, it is reasonable to hypothesize that these engineered NPs could act as "LDL-like" structures which can increase *in vivo* the clearance of A$\beta$ peptide from the biological fluids by capturing its soluble forms redirecting the peptide to the hepatic macrophages for destruction. Taking into consideration a recent study that evidenced the crucial role of blood peptide clearance in the decrease of the peptide toxicity in the brain (the so-called "*sink effect*"),[7] this capture could prevent the amyloid-beta aggregation process and its subsequent toxic effects on neuronal cells. In this context, these PEGylated NPs, which probably act toward the amyloid peptide through this sink effect mechanism, appear as very promising NPs to be tested *in vivo* on the AD model.

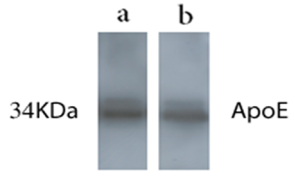


**Figure 10. Western blot analysis of Apo-E binding to P(MePEGCA-*co*-HDCA) NPs in control rat serum (a) or serum supplemented with A$\beta_{1-42}$ peptide (b). The antibody used specifically recognizes rat Apo-E.[24]**

## CONCLUSIONS

In summary, we have demonstrated that PEGylation of NPs can dramatically increase their affinity for A$\beta_{1-42}$ peptide monomers and soluble oligomers both

in solution and in the presence of serum proteins. As a result of collaborative hydrophilic and hydrophobic interactions between the PEG shell and $A\beta_{1-42}$ peptide, the latter could adsorb and aggregate at the surface of P(MePEGCA-*co*-HDCA) NPs. Moreover, following Apo-E adsorption from serum at the surface of these NPs, the peptide affinity is expected to be increased *in vivo*. $A\beta_{1-42}$ peptide binding to these nanoparticles did not affect complement activation further, and this could have important implications in both NP pharmacokinetic and anaphylactic reactions. We can speculate that these particles may act as a peptide sequester in the bloodstream, carrying the peptide to the liver where it could be enzymatically cleaved and degraded. With this in mind, the PEGylation could have a double-edged role: (*i*) drastically increase the blood half-life of the particles and (*ii*) increase the peptide adsorption onto the surface.

## MATERIALS AND EXPERIMENTS

**Materials.** Fetal bovine serum (FBS) was purchased from LonzaBioWhittaker (Verviers, Belgium). Poly[(hexadecyl cyanoacrylate)-*co*-rhodamine B cyanoacrylate-*co*-methoxypoly(ethylene glycol)$_{2000}$ cyanoacrylate] P(MePEGCA-*co*-RCA-*co*-HDCA) copolymers, poly[hexadecyl cyanoacrylate-*co*-methoxypoly(ethylene glycol)$_{2000}$ cyanoacrylate] P(MePEGCA-*co*-HDCA) copolymers, poly[(hexadecyl cyanoacrylate)-*co*-(rhodamine B cyanoacrylate)] P(HDCA-*co*-RCA), and poly(hexadecyl cyanoacrylate) (PHDCA) homopolymers were obtained following previously reported procedures.[26] $NaH_2PO_4$ (>99%) was purchased from Merck & Co. (Fontenay Sous Bois, France). $Na_2HPO_4$ (>98%) was obtained from Prolabo (Strasbourg, France), and thioflavin (99%), ammonium hydroxide ($NH_4OH$) 28.1% (m/V), Pluronic F-68 (99%), 1,1,1,3,3,3-hexafluoro-2-propanol (HFIP) (99.8%), dimethyl sulfoxide (99.5%), sodium dodecyl sulfate (SDS, 99%), acetic acid (99%), sodium acetate (99%), bovine serum albumin (BSA, 99%), and ethanolamine (99%) were purchased from Sigma-Aldrich (St. Quentin Fallavier, France). Sodium hydroxide (NaOH, 1 M) was obtained from VWR (Fontenay Sous Bois, France). Goat polyclonal anti-rat Apo-E (R-20) and mouse anti-goat-HRP antibodies were purchased from Santa-Cruz Biotechnology Inc. Anti-A$\beta$ antibody 6E10 was from Covance (Princeton, New Jersey). Invitrogen human $A\beta_{1-42}$ ultrasensitive ELISA kit was purchased from Fisher Scientific (Illkirch Cedex, France). Acetone was purchased at the highest grade from Carlo Erba (Val de Reuil, France).

**Nanoparticle Preparation.** Fluorescent and nonfluorescent PACA nanoparticles were prepared using P(MePEGCA-*co*-RCA-*co*-HDCA), P(MePEGCA-*co*-HDCA) copolymers, P(HDCA-*co*-RCA), and PHDCA homopolymer according to protocols recently published by our group.[26] The (co)polymer (10 mg) was dissolved in acetone (2 mL), and this solution was added dropwise to an aqueous solution 0.5% (w/v) of Pluronic F-68 (4 mL) under vigorous mechanical stirring. A milky suspension was observed almost instantaneously. Acetone was then evaporated under reduced pressure, and nanoparticles were purified by ultracentrifugation (150 000*g*, 1 h, 4 °C, Beckman Coulter, Inc.) in order to eliminate free polymer and the quasi-totality of Pluronic F-68. The supernatant was discarded, and the pellet was resuspended in the appropriate volume of deionized water to yield a 2.5 mg mL$^{-1}$ nanoparticle suspension.

PLA homopolymer and PLA-*b*-PEG block copolymers were synthesized by ring-opening polymerization.[28] D,L-Lactide (2.43 g, 16.9 mmol) and Sn(Oct)$_2$ (5.4 $\mu$L, 16.5 $\mu$mol) were added to a solution of methoxypoly(ethylene glycol) ($M_n$ = 2000 g·mol$^{-1}$, 500 mg, 0.24 mmol) in 5.2 mL of anhydrous toluene. The reaction mixture was degassed by bubbling nitrogen for 30 min and then stirred in a preheated oil bath at 115 °C for 5.5 h. The toluene was removed under reduced pressure, and the obtained product was dissolved into a minimum amount of THF and further precipitated twice in water and subsequently freeze-dried overnight to yield a white powder (conversion = 93%, $m$ = 1.7 g, $M_{n,NMR}$ = 12 200 g·mol$^{-1}$, $M_{n,SEC}$ = 12 400 g·mol$^{-1}$; $M_w/M_n$ = 1.12).

PLA and PLA-*b*-PEG nanoparticles were prepared as follows: 10 mg of polymer powder was dissolved in 4 mL of dichloromethane and added to 10 mL of an aqueous solution 1% (w/v) of Pluronic F-68. The resulting sample was physically mixed for 1 min and sonicated with a sonicator probe for 10 min (300 W). The organic solvent is then evaporated at room pressure and temperature under magnetic stirring, and nanoparticles were purified by ultracentrifugation (20 000*g*, 20 min) at 4 °C. The supernatant was discarded, and the pellet was resuspended in the appropriate volume of deionized water to yield a 2.5 mg·mL$^{-1}$ nanoparticle suspension. The same Pluronic F-68 concentration was used to prepare all nanoparticles in order to abolish the possible effect of Pluronic and to emphasize the role of covalently linked PEG on nanoparticle affinity to A$\beta$. In this text, P(PHDCA) and PLA nanoparticles will be referred to as non-PEGylated.

**Nanoparticle Characterization.** The nanoparticle diameter ($D_z$) was measured by dynamic light scattering (DLS) with a Nano ZS from Malvern (173° scattering angle) at 25 °C. The nanoparticle stability as a function of time using DLS measurements has been verified during their incubation at 37 °C in the buffer employed for capillary electrophoresis experiments. The nanoparticle surface charge was investigated by $\zeta$-potential measurement at 25 °C after dilution with 1 mM NaCl solution applying the Smoluchowski equation and using the same apparatus. The PEG chain density at the surface of PLA and PACA nanoparticles was obtained by a previous paper.[28] All of the values are presented in the Table 1. The distance between PEG chains was calculated as previously described.[31,32]

**Capillary Electrophoresis Experiments.** CE was performed on PA 800 instrument (Beckman Coulter, Roissy, France) using uncoated silica capillaries (Phymep, Paris) with an internal diameter of 50 $\mu$m and 50 cm total length (40 cm effective length was employed for the separation). All buffers were prepared with deionized water and were filtered through a 0.22 $\mu$m membrane (VWR) before use. Before analysis, the capillaries were preconditioned by the following rinsing sequence: 0.1 M NaOH for 5 min, 1 M NaOH for 5 min, and then deionized water for 5 min. The in-between-runs rinsing cycles were carried out by pumping sequentially through the capillary: water for 5 min, 50 mM SDS for 2 min (to inhibit the aggregation and subsequent peptide adsorption on the capillary wall),[33] and 0.1 M NaOH for 5 min. The samples were introduced into the capillary by hydrodynamic injection under 3.4 kPa. The capillary was thermostatted at 25 °C, and the samples were maintained at 37 °C by the storage sample module of the PA 800 apparatus. The separations were carried out at 16 kV with positive polarity at the inlet using 80 mM phosphate buffer ($NaH_2PO_4$/$Na_2HPO_4$) pH 7.4. The electrolyte was renewed after each run. The peptides were detected by a laser-induced fluorescence (LIF) detection system equipped with 3.5 mW argon ion laser with a wavelength excitation of 488 nm, the emission being collected through a 520 nm band-pass filter or by diode-array detector (DAD) at 190 nm. Peak areas were estimated using the 32 Karat software (Beckman Coulter).

Lyophilized $A\beta_{1-42}$ and HiLyte Fluor-labeled $A\beta_{1-42}$ peptide (ANASPEC, Le Perray en Yvelines, France) were dissolved in 0.16% (m/V) ammonium hydroxide aqueous solution to reach a concentration of 0.5 and 2 mg·mL$^{-1}$, respectively. The fluorescent and nonlabeled peptide solutions were then divided into aliquots individually stored at −20 °C, which were freshly defrosted prior to analysis.

To evaluate the interaction between the monomeric form of the $A\beta_{1-42}$ peptide and the nanoparticles, HiLyte Fluor-labeled

$A\beta_{1-42}$ peptide stock solution were diluted in 20 mM phosphate buffer ($NaH_2PO_4$) at pH 7.4 containing a 20 $\mu$M PEG solution or P(MePEGCA-*co*-RCA-*co*-HDCA), P(PHDCA), PEG-PLA, or PLA nanoparticle suspension to obtain final peptide concentrations of 5 $\mu$M. The samples were then incubated at 37 °C and analyzed by capillary electrophoresis several times as a function of time. The same protocol was followed with $A\beta_{1-42}$ peptide solution alone as a control.

A protocol to study the influence of polymeric NPs to the peptide aggregation kinetic was developed. An aggregating peptide solution was obtained as previously described.[30] Monomeric peptide was solubilized with a final concentration of 50 $\mu$M in phosphate buffer 20 mM ($NaH_2PO_4$), freeze-dried, and centrifuged 6000*g* for 20 min at room temperature. To ensure the aggregating behavior of the solution, ThT was employed. Under CE-LIF detection conditions, the anisotropic effect allowed a fluorescence emission from ThT when these molecules are exclusively linked to $\beta$-sheet structures. According to the studies of Kato *et al.*,[34] only the soluble oligomeric forms of the $A\beta_{1-42}$ peptide that contain $\beta$-sheet structure are susceptible to interact with ThT and are subsequently detected with the CE-LIF method. An alkaline buffer (pH 9.5, 0.2 M) of glycine/NaOH containing 10 $\mu$M of ThT was prepared, stored in the dark at 4 °C, and then used as the migration buffer. The samples were incubated at 4 °C, and subsequent separations were performed at 16 kV. The monomer form was not detected under these conditions.

To study the influence of polymeric NPs on this peptide aggregation kinetic, the same protocol to have an aggregating solution was followed. The obtained solution was analyzed by capillary electrophoresis with DAD detector in 20 mM phosphate buffer ($NaH_2PO_4$) pH 7.4 in the presence of 20 $\mu$M polymeric P(MePEGCA-*co*-HDCA) nanoparticles. Control experiments were performed without adding nanoparticles to the aggregating peptide solution.

These experiments allowed the quantification of the evolution of monomer or oligomer peak as a function of incubation time to be determined. Percent monomer or oligomer peaks was calculated as the ratio between the absolute peak area of the monomer or oligomer observed at $t$ = 0 and the one observed at each incubation time.

**Surface Plasmon Resonance Experiments.** The $A\beta_{1-42}$ peptide used for SPR experiments was prepared from a depsi-$A\beta_{1-42}$ peptide synthesized as previously described.[35] This depsi-peptide is much more soluble than the native peptide and has also a much lower propensity to aggregate, thus preventing the spontaneous formation of "seeds" in solution.[35] The native $A\beta_{1-42}$ peptide was then obtained from the depsi-peptide by a "switching" procedure involving a change in pH.[35] The $A\beta_{1-42}$ peptide solution obtained immediately after switching was shown to be free of seed. The $A\beta_{1-42}$ peptide obtained by this procedure is therefore in its original state, and for the sake of simplicity, it will be referred here to as the "monomer". Further characterizations, carried out earlier, indicated that the $A\beta$ "monomer" used for the present study gave no ThT signal and was unstructured as observed by circular dichroism.[36]

For binding studies, was used the ProteOn XPR36 (Biorad) apparatus, which has six parallel flow channels that can be used to uniformly immobilize strips of six ligands on the sensor surface. $A\beta_{1-42}$ monomers were immobilized in parallel-flow channels of a GLC sensor chip (Biorad) using amine-coupling chemistry.[37] Briefly, after surface activation, the peptide solutions (10 $\mu$M in acetate buffer pH 4.0) were injected for 5 min at a flow rate of 30 $\mu L \cdot min^{-1}$, and the remaining activated groups were blocked with ethanolamine, pH 8.0. The final immobilization level was about 3000 resonance units (1 RU = 1 pg protein/$mm^2$) for monomers. Bovine serum albumin (BSA) was immobilized too, in a parallel flow channel, as a reference protein. Another reference surface was prepared in parallel using the same immobilization procedure but without addition of the peptide (naked surface). Before performing experiments with nanoparticles, we previously checked that $A\beta$ species immobilized were binding with high affinity the anti-$A\beta$ antibody 6E10 (data not shown). PHDCA and P(HDCA-*co*-MePEGCA) NPs were then injected at different concentrations (0.3 to 20 $\mu$M) and flowed onto the chip surfaces for 3 min at a flow rate of 30 $\mu$L/min at 30 °C in PBST (phosphate buffer saline + 0.005% Tween 20, pH 7.4). A second set of experiments (2000 RU) were performed using P(MePEGCA-*co*-RCA-*co*-HDCA) with increased contact time (10 min) to calculate the affinity constant.

**Thioflavin T Aggregation Assay.** $A\beta_{1-42}$ was dissolved in hexafluorisopropanol (HFIP) at a final concentration of 1 $mg \cdot mL^{-1}$, sampled, and allowed to evaporate. For coaggregation experiments, the peptide film was first dissolved in DMSO and sonicated in a bath sonicator for 10 min. Subsequently, $A\beta_{1-42}$ was diluted in phosphate buffer saline (20 mM sodium phosphate buffer, pH 7.4, containing 137 mM NaCl) to a final concentration of 50 $\mu$M. This mixture was aggregated in the presence or absence of PHDCA or P(MePEGCA-*co*-HDCA) NPs for 24 h at 37 °C. At each point of analysis (0.5, 1, 2, 4, 6, 24 h), aggregated $A\beta_{1-42}$ was diluted to a final concentration of 5 $\mu$M into 50 mM glycine buffer at pH 7.4 containing 10 $\mu$M ThT. Fluorescence was measured in 96-well nonbinding plates (Greiner Bio One, Frickenhausen, Germany) using a Fluostar Omega microplate reader at an excitation wavelength of 450 nm and emission at 485 nm.

**Confocal Laser Scanning Microscopy Experiments.** Observations were made by sequential acquisition with a Zeiss LSM-510 confocal scanning laser microscope equipped with a 30 mW argon laser and 1 mW helium neon laser, using a Plan-Apochromat 63× objective lens (NA 1.40, oil immersion). Red fluorescence was observed with a long-pass 560 nm emission filter and under a 543 nm laser illumination. Green fluorescence was observed with a band-pass 505 and 550 nm emission filter and under a 488 nm laser illumination. The pinhole diameter was set at 61 $\mu$m, giving an optical section thickness of 0.6 $\mu$m. Stacks of images were collected every 0.3 $\mu$m along the $z$ axis. Twelve bit numerical images were acquired with LSM 510 software version 3.2.

The interaction between the polymeric nanoparticles and the $A\beta_{1-42}$ peptide was investigated by confocal laser scanning microscopy (CLSM) using HiLyte Fluor-labeled $A\beta_{1-42}$ peptide and rhodamine-labeled P(MePEGCA-*co*-RCA-*co*-HDCA) and P(HDCA-*co*-RCA) NPs. The $A\beta_{1-42}$ peptide aliquots were defrosted, immediately diluted with 20 mM phosphate buffer, and incubated with 20 $\mu$M nanoparticle suspension to reach a final peptide concentration of 10 $\mu$M. After 12 h of incubation at 37 °C, a 10 $\mu$L deposit of the sample on glass coverslips was analyzed by CLSM.

**Molecular Modeling Experiments.** For the docking calculations, we used a polymeric chain with the 16 PEG (polyethylene glycol) units (it is the maximum length of the PEG chain allowable for the flexible docking calculations, *i.e.*, a maximum 50 rotatable bonds) and 24 PE (polyethylene) units as ligands and a solution structures (PDB ID: 1IYT)[11] of the $A\beta_{1-42}$ peptide as a receptor. For the docking calculations, default values of parameters were used by means of the GLIDE program[38,39] of the Schrödinger package.[40] The receptor box for the docking conformational search was centered at the receptor with a size of 50 × 50 × 50 Å using partial atomic charges for the receptor and ligand from the OPLS2005 force field.[41,42] The grid maps were created with no van der Waals radius and charge scaling for the atoms of the receptor. Flexible docking in standard (SP) and extra (XP) precision was used for the PEG and PE ligands. The potential for nonpolar parts of the ligands was softened by scaling the van der Waals radii by a factor of 1.0 for atoms of the ligands with partial atomic charges less than specified cutoff of 0.15. The 5000 poses were kept per ligand for the initial docking stage with scoring window of 100 kcal $mol^{-1}$ for keeping initial poses, and the best 400 poses were kept per ligand for energy minimization. The ligand poses with rms deviations less than 0.5 Å and maximum atomic displacement less than 1.3 Å were discarded as duplicates. For 50 ligand poses with the best docking score, post-docking minimizations were performed. Subsequent structural analyses were done using the MAESTRO viewer of the Schrödinger package.[43]

For molecular dynamics simulations, the $A\beta_{1-42}$-PEG (or PE) systems were solvated by more than 4800 TIP3P[44] water molecules in a box (82 × 68 × 96 Å) using the LEAP[45] program of the Amber 10 program package.[46] The $A\beta_{1-42}$ peptide was

treated with the standard AMBER 99 force field with the "Stony Brook" (SB) modification to ff99 backbone torsions, and for the PEG and PE chains, the parameters were derived from the GAFF force field. The ionization states of the ionizing residues of $A\beta_{1-42}$ were predicted by the PropKa program,[47,48] considering an *in vivo* pH of 7. Terminal and side-chain ionizing groups (amino and carboxyl) of $A\beta_{1-42}$ were treated in their ionized configurations (as $-NH^{3+}$ or $-COO^{-}$) in all MD simulations. The Berendsen algorithm[49] for the temperature and pressure coupling, with coupling constants of $\tau_t = 1.0$ ps and $\tau_p = 1.0$ ps, was used at a constant temperature (300 K) and pressure (101.325 kPa) employing the PMEMD module. Periodic boundary conditions were used together with the particle-mesh Ewald (PME)[46] method for treating long-range electrostatics. A time step of 1.0 fs, with the SHAKE algorithm[50] to constrain bonds involving hydrogens, was used along simulations with a 10 Å nonbonded cutoff, and the nonbonded pairlist was updated every 20 time step. The simulations, preceded by initial minimizations (300 steps), were carried out over 20 ns, and coordinates were saved for analysis every 1 ps. The MD trajectories were analyzed by the VMD package[51] and the DSSP program.[52]

**Complement Activation Analyses.** First, P(HDCA-*co*-MePEGCA) nanoparticles (64 $\mu$g) were incubated with the $A\beta_{1-42}$ peptide (4.9 $\mu$g) in a total volume of 1 mL of saline for 24 h at 37 °C. $A\beta$-bound nanoparticles were pelleted by centrifugation at 100 000*g* for 1 h at 4 °C. After removing the supernatant, the pellet was washed with deionized water and concentrated by centrifugation. Finally, the pellet was resuspended in an appropriated volume of physiological saline and used immediately for complement activation testing. P(HDCA-*co*-MePEGCA) NP-containing sample without $A\beta$ peptide was used as control, and it was processed as above, where the $A\beta$ peptide was replaced with an equal volume of deionized water.

Blood was drawn from healthy volunteers according to approved local protocols (Moghimi's group, University of Copenhagen). Blood was allowed to clot at room temperature, and serum was prepared, aliquoted, and stored at −80 °C. Serum samples were thawed and kept at 4 °C before incubation with test reagents.

To measure complement activation *in vitro*, we compared $A\beta$-bound P(HDCA-*co*-MePEGCA) NP- and unbound P(HDCA-*co*-MePEGCA) NP-induced rise of serum complement activation products Bb, C4d, C5a, and SC5b-9 using respective Quidel's ELISA kits according to the manufacturer's protocols, as described previously.[53−55] The reaction was started by adding the required amount of $A\beta$-bound P(HDCA-*co*-MePEGCA) NPs or unbound P(HDCA-*co*-MePEGCA) NPs to undiluted serum (NPs/serum volume ratio, 1:4) in Eppendorf tubes (in triplicate) in a shaking water bath at 37 °C for 30 min. The final concentration of P(HDCA-*co*-MePEGCA) NPs was 0.4 mg·mL$^{-1}$ of serum. Reactions were terminated by 20-fold dilution with "sample diluents" provided with assay kit supplemented with 25 mM EDTA for Bb, C4d, and SC5b-9 detection, whereas a 200-fold dilution was made prior to C5a measurement. Control serum incubations contained saline (the same volume as nanoparticles) for assessing background levels of complement activation products. Zymosan (1 mg·mL$^{-1}$, final concentration) and heat-aggregated IgG (5 mg·mL$^{-1}$, final concentration) were used as positive controls for alternative and calcium-sensitive pathways, respectively. The level of the complement activation products was then measured by the respective ELISA kits and compared with control incubations in the absence of nanoparticles. For quantification of complement activation products, standard curves were constructed using the assigned concentration of each respective standard supplied by the manufacturer and validated. The slope, intercept, and correlation coefficient of the derived best-fit line for Bb, C4d, C5a, and SC5b-9 standard curves was within the manufacturer's specified range. The efficacy of $A\beta$ bound to P(HDCA-*co*-MePEGCA) NPs and unbound NPs was established by comparison with baseline levels using paired *t* test, and correlations between two variables were analyzed by linear regression. The result of a typical experiment from one blood donor is presented.

**$A\beta_{1-42}$ Peptide−NP Interaction in Serum.** The ability of the nanoparticle to interact with the $A\beta$ peptide in a biological sample was studied in fetal bovine serum (Lonza). NPs and fluorescently labeled peptide (HiLyte Fluor-labeled $A\beta_{1-42}$) were incubated at a final concentration of 100 and 5 $\mu$M, respectively, in 443 $\mu$L of serum. The samples were then stored on an orbital shaking plate at 37 °C. After 7 h, the tubes were centrifuged in mild conditions (15 000*g* for 1.5 h at 4 °C) in order to remove the NPs and the adsorbed entities without desorbing adsorbed proteins. The resulting supernatant was directly analyzed with a luminescence spectrometer (LS50 B, Perkin-Elmer) with $\lambda_{ex}$ of 503 nm in a Hellma Analytics quartz cuvette (104.003F-QS). Samples of peptide alone in serum and serum alone were employed as controls.

The ability of the PEGylated nanoparticles to interact with the peptide in biological media was further investigated by ELISA. NPs and nonfluorescent $A\beta_{1-42}$ peptide (aliquoted in $NH_4Cl$ 1% w/w) were incubated at a final concentration of 0.1 and 0.05 $\mu$M, respectively, in 1.0 mL of FBS. Again, after 7 h, the tubes were centrifuged at 15 000*g* for 1.5 h at 4 °C to remove NPs and the adsorbed entities. The supernatants were analyzed by ELISA assay (human $A\beta_{1-42}$ ultrasensitive, Invitrogen). The absorbance values were normalized with a sample of peptide. Experiments were performed in triplicate, and the results were the mean ± SD. Statistical comparisons of peptide levels were done by Student's tests.

**Apo-E Adsorption on the NPs.** A total of 350 $\mu$L of P(MePEGCA-*co*-HDCA) nanoparticle suspension (20 mg·mL$^{-1}$) was incubated in 1.75 mL of Sprague−Dawley rat serum (Charles River Laboratories) for 20 min at 37 °C with or without $A\beta_{1-42}$. Plasma proteins adsorbed onto the nanoparticles were separated from bulk serum by centrifugation at 15 000*g* for 1.5 h at 4 °C. The supernatant serum was discarded, and the pellet was extensively washed with water by centrifugation (15 000*g* for 1.5 h at 4 °C) to remove the excess serum. After the centrifugation, the plasma protein adsorbed nanoparticles were resuspended in 100 $\mu$L of solution containing 2.5% sodium dodecyl sulfate (SDS) and 30 mM 1,4-dithioerythritol (DTE). The suspension was incubated at 50 °C for 2 h to detach the adsorbed proteins from the nanoparticles.[56] After centrifugation at 15 000*g* for 1 h at 4 °C, Bradford assay was applied to quantify the amount proteins in the final supernatant. A total of 40 $\mu$g of proteins was migrated on a 12% SDS polyacrylamide gel and electrophoretically transferred to a nitrocellulose membrane. Blots were blocked with BSA 5% (w/v) in Tris buffer saline. Then the blots were extensively washed and incubated with an apolipoprotein-specific antibody overnight at 4 °C, followed by a peroxidase-conjugated anti-goat IgG as a secondary antibody. The immunoreactive bands were visualized by an enhanced chemoluminescence system (Amersham Bioscience).

*Conflict of Interest:* The authors declare no competing financial interest.

*Acknowledgment.* The research leading to these results has received funding from the European Community's Seventh Framework Program (FP7/2007-2013) under agreement No. 212043. The CNRS and the French Ministry of Research are further acknowledged for financial support. J.K. and I.T. also acknowledge the financial support from the Scientific Grant Agency of the Ministry of Education of Slovak Republic and Slovak Academy of Sciences (the project VEGA-02/0176/09). S.M.M. also acknowledges financial support by the Danish Agency for Science, Technology, and Innovation (Det Strategiske Forskningsråd), reference 2106-08-0081.

*Supporting Information Available:* Figures S1 and S2. Surface plasmon resonance experiments: controls and labeled NPs; Figure S3. Confocal microscopy images of interaction between peptide and NPs; Figure S4. CE-LIF experiments: control of peptide aggregation; Figure S5. Root-mean-square deviation (rmsd) of the Cα carbons of the $A\beta_{1-42}$ backbone in the presence of PEG and PE. This material is available free of charge *via* the Internet at http://pubs.acs.org.

## REFERENCES AND NOTES

1. Querfurth, H. W.; LaFerla, F. M. Alzheimer's Disease. *N. Engl. J. Med.* **2010**, *362*, 329–344.

2. Aliev, G.; Smith, M. A.; de la Torre, J. C.; Perry, G. Mitochondria as a Primary Target for Vascular Hypoperfusion and Oxidative Stress in Alzheimer's Disease. *Mitochondrion* **2004**, *4*, 649–663.
3. Gralle, M.; Botelho, M. G.; Wouters, F. S. Neuroprotective Secreted Amyloid Precursor Protein Acts by Disrupting Amyloid Precursor Protein Dimers. *J. Biol. Chem.* **2009**, *284*, 15016–15025.
4. Townsend, M.; Mehta, T.; Selkoe, D. J. Soluble A$\beta$ Inhibits Specific Signal Transduction Cascades Common to the Insulin Receptor Pathway. *J. Biol. Chem.* **2007**, *282*, 33305–33312.
5. Chow, V. W.; Mattson, M. P.; Wong, P. C.; Gleichmann, M. An Overview of APP Processing Enzymes and Products. *NeuroMol. Med.* **2010**, *12*, 1–12.
6. Pierrot, N.; Octave, J. Processing of Amyloid Precursor Protein and Amyloid Peptide Neurotoxicity. *Curr. Alzheimer Res.* **2008**, *5*, 92–99.
7. Sutcliffe, J. G.; Hedlund, P. B.; Thomas, E. A.; Bloom, F. E.; Hilbush, B. S. Peripheral Reduction of Beta-Amyloid Is Sufficient To Reduce Brain Beta-Amyloid: Implications for Alzheimer's Disease. *J. Neurosci. Res.* **2011**, *89*, 808–814.
8. Deane, R.; Sagare, A.; Hamm, K.; Parisi, M.; Lane, S.; Finn, M. B.; Holtzman, D. M.; Zlokovic, B. V. ApoE Isoform–Specific Disruption of Amyloid B Peptide Clearance from Mouse Brain. *J. Clin. Invest.* **2008**, *118*, 4002–4013.
9. Sagare, A.; Deane, R.; Bell, R. D.; Johnson, B.; Hamm, K.; Pendu, R.; Marky, A.; Lenting, P. J.; Wu, Z.; Zarcone, T.; *et al.* Clearance of Amyloid-Beta by Circulating Lipoprotein Receptors. *Nat. Med.* **2007**, *13*, 1029–1031.
10. Zlokovic, B. V. Clearing Amyloid through the Blood–Brain Barrier. *J. Neurochem.* **2004**, *89*, 807–811.
11. Crescenzi, O.; Tomaselli, S.; Guerrini, R.; Salvadori, S.; D'Ursi, A. M.; Temussi, P. A.; Picone, D. Solution Structure of the Alzheimer Amyloid Beta-Peptide (1–42) in an Apolar Microenvironment. Similarity with a Virus Fusion Domain. *Eur. J. Biochem.* **2002**, *269*, 5642–6548.
12. De Kimpe, L.; Scheper, W. From Alpha to Omega with A$\beta$: Targeting the Multiple Molecular Appearances of the Pathogenic Peptide in Alzheimer's Disease. *Curr. Med. Chem.* **2010**, *17*, 198–212.
13. Allaman, I.; Gavillet, M.; Belanger, M.; Laroche, T.; Viertl, D.; Lashuel, H. A.; Magistretti, P. J. Amyloid-Beta Aggregates Cause Alterations of Astrocytic Metabolic Phenotype: Impact on Neuronal Viability. *J. Neurosci.* **2010**, *30*, 3326–3338.
14. Garcia-Matas, S.; de Vera, N.; Aznar, A. O.; Marimon, J. M.; Adell, A.; Planas, A. M.; Cristofol, R.; Sanfeliu, C. *In Vitro* and *In Vivo* Activation of Astrocytes by Amyloid-Beta Is Potentiated by Pro-oxidant Agents. *J. Alzheimers Dis.* **2010**, *20*, 229–245.
15. Cizas, P.; Budvytyte, R.; Morkuniene, R.; Moldovan, R.; Broccio, M.; Losche, M.; Niaura, G.; Valincius, G.; Borutaite, V. Size-Dependent Neurotoxicity of Beta-Amyloid Oligomers. *Arch. Biochem. Biophys.* **2010**, *496*, 84–92.
16. Maezawa, I.; Zimin, P. I.; Wulff, H.; Jin, L. W. Amyloid-Beta Protein Oligomer at Low Nanomolar Concentrations Activates Microglia and Induces Microglial Neurotoxicity. *J. Biol. Chem.* **2011**, *286*, 3693–3706.
17. Brambilla, D.; Le Droumaguet, B.; Nicolas, J.; Hashemi, S. H.; Wu, L.-P.; Moghimi, S. M.; Couvreur, P.; Andrieux, K. Nanotechnologies for Alzheimer's Disease: Therapy, Diagnosis and Safety Issues. *Nanomedicine: Nanotechnol., Biol. Med.* **2011**, *7*, 521–540.
18. Costa, M.; Ortiz, A. M.; Jorquera, J. I. Therapeutic Albumin Binding to Remove Amyloid-Beta. *J. Alzheimers Dis.* **2012**, *29*, 159–170.
19. Viet, M. H.; Ngo, S. T.; Lam, N. S.; Li, M. S. Inhibition of Aggregation of Amyloid Peptides by Beta-Sheet Breaker Peptides and Their Binding Affinity. *J. Phys. Chem. B* **2011**, *115*, 7433–7446.
20. Couvreur, P.; Kante, B.; Roland, M.; Guiot, P.; Bauduin, P.; Speiser, P. Polycyanoacrylate Nanocapsules as Potential Lysosomotropic Carriers: Preparation, Morphological and Sorptive Properties. *J. Pharm. Pharmacol.* **1979**, *31*, 331–332.
21. Vauthier, C.; Dubernet, C.; Fattal, E.; Pinto-Alphandary, H.; Couvreur, P. Poly(alkylcyanoacrylates) as Biodegradable Materials for Biomedical Applications. *Adv. Drug Delivery Rev.* **2003**, *55*, 519–548.
22. Reddy, L. H.; Couvreur, P. Nanotechnology for Therapy and Imaging of Liver Diseases. *J. Hepatol.* **2011**, *55*, 1461–1466.
23. Service, R. F. Nanotechnology. Nanoparticle Trojan Horses Gallop from the Lab into the Clinic. *Science* **2010**, *330*, 314–315.
24. Kim, H. R.; Andrieux, K.; Gil, S.; Taverna, M.; Chacun, H.; Desmaele, D.; Taran, F.; Georgin, D.; Couvreur, P. Translocation of Poly(ethylene glycol-*co*-hexadecyl)cyanoacrylate Nanoparticles into Rat Brain Endothelial Cells: Role of Apolipoproteins in Receptor-Mediated Endocytosis. *Biomacromolecules* **2007**, *8*, 793–799.
25. Peracchia, M. T.; Harnisch, S.; Pinto-Alphandary, H.; Gulik, A.; Dedieu, J. C.; Desmaele, D.; d'Angelo, J.; Muller, R. H.; Couvreur, P. Visualization of *In Vitro* Protein-Rejecting Properties of PEGylated Stealth Polycyanoacrylate Nanoparticles. *Biomaterials* **1999**, *20*, 1269–1275.
26. Brambilla, D.; Nicolas, J.; Le Droumaguet, B.; Andrieux, K.; Marsaud, V.; Couraud, P. O.; Couvreur, P. Design of Fluorescently Tagged Poly(alkyl cyanoacrylate) Nanoparticles for Human Brain Endothelial Cell Imaging. *Chem. Commun.* **2010**, *46*, 2602–2604.
27. Brambilla, D.; Verpillot, R.; Taverna, M.; De Kimpe, L.; Le Droumaguet, B.; Nicolas, J.; Canovi, M.; Gobbi, M.; Mantegazza, F.; Salmona, M.; *et al.* New Method Based on Capillary Electrophoresis with Laser-Induced Fluorescence Detection (CE-LIF) To Monitor Interaction between Nanoparticles and the Amyloid-Beta Peptide. *Anal. Chem.* **2010**, *82*, 10083–10089.
28. Brambilla, D.; Souguir, H.; Nicolas, J.; Mackiewicz, N.; Verpillot, R.; Le Droumaguet, B.; Taverna, M.; Couvreur, P.; Andrieux, K. Colloidal Properties of Biodegradable Nanoparticles Influence Interaction with Amyloid-Beta Peptide. *J. Biotechnol.* **2011**, *156*, 338–340.
29. Peracchia, M. T.; Fattal, E.; Desmaele, D.; Besnard, M.; Noel, J. P.; Gomis, J. M.; Appel, M.; d'Angelo, J.; Couvreur, P. Stealth PEGylated Polycyanoacrylate Nanoparticles for Intravenous Administration and Splenic Targeting. *J. Controlled Release* **1999**, *60*, 121–128.
30. Sabella, S.; Quaglia, M.; Lanni, C.; Racchi, M.; Govoni, S.; Caccialanza, G.; Calligaro, A.; Bellotti, V.; De Lorenzi, E. Capillary Electrophoresis Studies on the Aggregation Process of Beta-Amyloid 1–42 and 1–40 Peptides. *Electrophoresis* **2004**, *25*, 3186–3194.
31. Gref, R.; Luck, M.; Quellec, P.; Marchand, M.; Dellacherie, E.; Harnisch, S.; Blunk, T.; Muller, R. H. 'Stealth' Corona-Core Nanoparticles Surface Modified by Polyethylene Glycol (PEG): Influences of the Corona (PEG Chain Length and Surface Density) and of the Core Composition on Phagocytic Uptake and Plasma Protein Adsorption. *Colloids Surf., B* **2000**, *18*, 301–313.
32. Gref, R.; Minamitake, Y.; Peracchia, M. T.; Trubetskoy, V.; Torchilin, V.; Langer, R. Biodegradable Long-Circulating Polymeric Nanospheres. *Science* **1994**, *263*, 1600–1603.
33. Han, Y.; He, C.; Cao, M.; Huang, X.; Wang, Y.; Li, Z. Facile Disassembly of Amyloid Fibrils Using Gemini Surfactant Micelles. *Langmuir* **2010**, *26*, 1583–1587.
34. Kato, M.; Kinoshita, H.; Enokita, M.; Hori, Y.; Hashimoto, T.; Iwatsubo, T.; Toyo'oka, T. Analytical Method for Beta-Amyloid Fibrils Using CE-Laser Induced Fluorescence and Its Application to Screening for Inhibitors of Beta-Amyloid Protein Aggregation. *Anal. Chem.* **2007**, *79*, 4887–4891.
35. Taniguchi, A.; Sohma, Y.; Hirayama, Y.; Mukai, H.; Kimura, T.; Hayashi, Y.; Matsuzaki, K.; Kiso, Y. "Click Peptide": pH-Triggered *In Situ* Production and Aggregation of Monomer A$\beta$1–42. *ChemBioChem* **2009**, *10*, 710–715.
36. Beeg, M.; Stravalaci, M.; Bastone, A.; Salmona, M.; Gobbi, M. A Modified Protocol To Prepare Seed-Free Starting Solutions of Amyloid-Beta (A$\beta$) and A$\beta$ from the Corresponding Depsipeptides. *Anal. Biochem.* **2011**, *411*, 297–299.

37. Stravalaci, M.; Beeg, M.; Salmona, M.; Gobbi, M. Use of Surface Plasmon Resonance To Study the Elongation Kinetics and the Binding Properties of the Highly Amyloidogenic A$\beta$1−42 Peptide, Synthesized by Depsi-Peptide Technique. *Biosens. Bioelectron.* **2011**, *26*, 2772–2775.
38. Friesner, R. A.; Banks, J. L.; Murphy, R. B.; Halgren, T. A.; Klicic, J. J.; Mainz, D. T.; Repasky, M. P.; Knoll, E. H.; Shelley, M.; Perry, J. K.; *et al.* Glide: A New Approach for Rapid, Accurate Docking and Scoring. 1. Method and Assessment of Docking Accuracy. *J. Med. Chem.* **2004**, *47*, 1739–1749.
39. Friesner, R. A.; Murphy, R. B.; Repasky, M. P.; Frye, L. L.; Greenwood, J. R.; Halgren, T. A.; Sanschagrin, P. C.; Mainz, D. T. Extra Precision Glide: Docking and Scoring Incorporating a Model of Hydrophobic Enclosure for Protein−Ligand Complexes. *J. Med. Chem.* **2006**, *49*, 6177–6196.
40. *Glide*, version 5.5; Schrodinger, LLC: New York, 2009.
41. Jorgensen, W. L.; Maxwell, D. S.; Tirado-Rives, J. Development and Testing of the Opls All-Atom Force Field on Conformational Energetics and Properties of Organic Liquids. *J. Am. Chem. Soc.* **1996**, *118*, 11225–11236.
42. Kaminski, G. A.; Friesner, R. A.; Tirado-Rives, J.; Jorgensen, W. L. Evaluation and Reparametrization of the Opls-Aa Force Field for Proteins *via* Comparison with Accurate Quantum Chemical Calculations on Peptides. *J. Phys. Chem. B* **2001**, *105*, 6474–6487.
43. *MAESTRO*, version 9.0; Schrodinger, LLC: New York, 2009.
44. Jorgensen, W. L.; Chandrasekhar, J.; Madura, J. D.; Impey, R. W.; Klein, M. L. Comparison of Simple Potential Functions for Simulating Liquid Water. *J. Chem. Phys.* **1983**, *79*, 926–935.
45. Schafmeister, C. E. A. F.; Ross, W. S.; Romanovski, V. *LEAP*; University of California, San Francisco, 1995.
46. Case, D. A.; Darden, T. A.; Cheatham, T. E., III; Simmerling, C. L.; Wang, J.; Duke, R. E.; Luo, R.; Crowley, M.; Walker, R. C.; Zhang, W.; *et al. AMBER 10*; University of California, San Francisco, 2008.
47. Bas, D. C.; Rogers, D. M.; Jensen, J. H. Very Fast Prediction and Rationalization of p$K_a$ Values for Protein−Ligand Complexes. *Proteins: Struct., Funct., Bioinf.* **2008**, *73*, 765–783.
48. Li, H.; Robertson, A. D.; Jensen, J. H. Very Fast Empirical Prediction and Rationalization of Protein p$K_a$ Values. *Proteins: Struct., Funct., Bioinf.* **2005**, *61*, 704–721.
49. Berendsen, H. J. C.; Postma, J. P. M.; Vangunsteren, W. F.; Dinola, A.; Haak, J. R. Molecular-Dynamics with Coupling to an External Bath. *J. Chem. Phys.* **1984**, *81*, 3684–3690.
50. Ryckaert, J. P.; Ciccotti, G.; Berendsen, H. J. C. Numerical Integration of the Cartesian Equations of Motion of a System with Constraints; Molecular Dynamics of *n*-Alkanes. *J. Comput. Phys.* **1977**, *23*, 327–341.
51. Humphrey, W.; Dalke, A.; Schulten, K. VMD: Visual Molecular Dynamics. *J. Mol. Graph.* **1996**, *14*, 27–28.
52. Kabsch, W.; Sander, C. Dictionary of Protein Secondary Structure: Pattern Recognition of Hydrogen-Bonded and Geometrical Features. *Biopolymers* **1983**, *22*, 2577–2637.
53. Hamad, I.; Hunter, A. C.; Szebeni, J.; Moghimi, S. M. Poly(ethylene glycol)S Generate Complement Activation Products in Human Serum through Increased Alternative Pathway Turnover and a Masp-2-Dependent Process. *Mol. Immunol.* **2008**, *46*, 225–232.
54. Moghimi, S. M.; Hamad, I.; Al-Hanbali, O.; Hunter, A. C.; Rutt, K. J.; Andresen, T. L. Distinct Polymer Architecture Mediates Switching of Complement Activation Pathways at the Nanosphere−Serum Interface: Implications for Stealth Nanoparticle Engineering. *ACS Nano* **2010**, *4*, 6629–6638.
55. Moghimi, S. M.; Hamad, I.; Andresen, T. L.; Jorgensen, K.; Szebeni, J. Methylation of the Phosphate Oxygen Moiety of Phospholipid−Methoxy(polyethylene glycol) Conjugate Prevents PEGylated Liposome-Mediated Complement Activation and Anaphylatoxin Production. *FASEB J.* **2006**, *20*, 2591–2593.
56. Allemann, E.; Gravel, P.; Leroux, J. C.; Balant, L.; Gurny, R. Kinetics of Blood Component Adsorption on Poly(D,L-lactic acid) Nanoparticles: Evidence of Complement C3 Component Involvement. *J. Biomed. Mater. Res.* **1997**, *37*, 229–334.